Theoretical study on the mechanism and kinetics of acetaldehyde and hydroperoxyl radical: An important atmospheric reaction

ARTICLE *in* CHEMICAL PHYSICS LETTERS · SEPTEMBER 2013

Impact Factor: 1.9 · DOI: 10.1016/j.cplett.2013.07.065

4 AUTHORS, INCLUDING:

Morteza Vahedpour
University of Zanjan
45 PUBLICATIONS **185** CITATIONS

SEE PROFILE

Chemical Physics Letters 583 (2013) 190–197

Contents lists available at ScienceDirect

Chemical Physics Letters

journal homepage: www.elsevier.com/locate/cplett

Theoretical study on the mechanism and kinetics of acetaldehyde and hydroperoxyl radical: An important atmospheric reaction

Solaleh Farnia [a], Morteza Vahedpour [a], Mostafa Abedi [b], Hossein Farrokhpour [b,*]

[a] Department of Chemistry, University of Zanjan, Zanjan 38791-45371, Iran
[b] Department of Chemistry, Isfahan University of Technology, Isfahan 84156-83111, Iran

ARTICLE INFO

Article history:
Received 25 February 2013
In final form 26 July 2013
Available online 12 August 2013

ABSTRACT

A systematic theoretical study was performed on the mechanism and kinetics of the atmospheric reaction of acetaldehyde (CH_3CHO) and hydroperoxyl radical (HO_2) in the gas phase. The DFT-B3LYP/6-311++G(3df,3pd) and CCSD(T)/6-311++G(d,p) methods were employed for calculations. Based on the calculations, this reaction leads to four different products through radical addition and hydrogen abstraction mechanisms which are very important in atmospheric and combustion chemistry. The favorable reaction paths begin with α-hydroxyethylperoxy radical, $CH_3CH(OO)OH$, in a exothermic process and finally leads to the product P1 ($CH_3COOH + OH$). The overall rate constants for favorite reaction paths have been calculated at different temperatures (200–2500 K).

1. Introduction

Large quantities of volatile organic compounds (VOCs) are emitted into the troposphere from anthropogenic and biogenic sources [1]. The classes of oxygen-containing VOCs considered are aldehydes. Acetaldehyde is an aldehyde that acts as a reactive organic contaminant in atmosphere. Amongst VOCs, acetaldehyde is responsible for offensive odors, affects the nervous system and is suspected to be carcinogenic. Therefore, controlling this pollutant has attracted much interest in recent years [2–4]. Acetaldehyde is a colorless, flammable liquid and volatile at ambient temperature and pressure. It can be used in a wide variety of chemical reactions, many of which are useful in commercial processes. The dominant atmospheric removal mechanism for acetaldehyde during daylight hours is by photolysis and oxidation by hydroxyl radicals [5].

The reaction of acetaldehyde with hydroperoxyl radical also plays a significant role, mainly in polluted atmospheres in which the ratio between HO_2 and HO radicals is high [5]. As described by Eq. (1), the addition of hydroperoxyl to acetaldehyde could produce the α-hydroxyethylperoxy radical [6] which is decomposed to α-hydroxyethyl radical and O_2.

$$HO_2 + CH_3CHO \rightarrow CH_3CH(OO)OH \rightarrow CH_3CHOH + O_2 \quad (1)$$

There are different theoretical and experimental papers in the literature on the different aspects of the reactions between VOCs and the HO_X family [7–11]. Anglada and Domingo [5] studied the mechanism of the reaction between the HCHO and HO_2 radical, theoretically; and Da Silva and Bozzelli [10] investigated the role of the α-hydroxyethylperoxy radical in the reactions of acetaldehyde and vinyl alcohol with HO_2. Tomas et al. [6] have also studied the kinetics and thermodynamic of a part of the $HO_2 + CH_3CHO$ reaction mechanism, experimentally, using flash photolysis UV absorption techniques.

A further interest in the reaction between acetaldehyde and hydroperoxyl radical arises from its importance in combustion processes through the following reactions

$$HO_2 + CH_3CHO \rightarrow CH_3CO + H_2O_2 \quad (2)$$

$$HO_2 + CH_3CHO \rightarrow CH_2CHO + H_2O_2 \quad (3)$$

The main objective of this work is to perform a detailed theoretical study on the $HO_2 + CH_3CHO$ reaction with the aim of clarifying the reaction mechanism. The kinetic studies have been reported in the 200–2500 K temperature range.

2. Theoretical detail of calculations

We present different theoretical approaches in this study. In short, calculations of molecular geometries were carried out by employing the unrestricted hybrid density functional B3LYP [12,13] method in connection with the 6-311++G(3df,3pd) [14] basis set. At this level of theory, harmonic frequencies were calculated for all stationary points in order to clarify the nature (minima or transition state) of corresponding stationary points and gain zero-point energies plus thermodynamic contributions to the enthalpy and Gibbs free energies. Moreover, to confirm whether the obtained transition states connect the right complexes, the intrinsic reaction coordinate (IRC) [15–18] calculations

* Corresponding author.
E-mail address: farrokhphossein@gmail.com (H. Farrokhpour).

0009-2614/$ - see front matter © 2013 Elsevier B.V. All rights reserved.
http://dx.doi.org/10.1016/j.cplett.2013.07.065

were performed. Relative energies were calculated at the optimized B3LYP geometries, single-point CCSD(T) [19,20] by using 6-311++G(d,p) basis set. In addition, the basis set superposition error (BSSE) was also calculated at this level of theory according to the counterpoise method by Boys and Bernardi [21]. All computations were performed with the Gaussian 03 programs [22]. Bonding natures of several complexes of interest were analyzed by Bader's theory [23], the atoms in molecules (AIM). This analysis was performed at the B3LYP approach by using the AIMAll package (Version 12.06.03) [24]. Finally, kinetic studies were carried out by using the Rice–Ramsperger–Kassel–Marcus (RRKM) [25–30] and conventional transition state theories on the most favorable pathways of reaction.

3. Results and discussion

All of the elementary reactions observed in this work begin with the formation of a pre-reactive complex that is remarked by the prefix Cr and various numbers to distinguish one from each other. The prefix TS and a number is designated for the transition states. Some of intermediates are regarded by the prefix IM followed by a number. Before releasing the products, there are also complexes which are noted with the prefix Cp and a number. Figures 1 and 2 represent the structural parameters of the stationary points of reactants, pre-complexes, transition sates, intermediate and products which are found in the present work. In addition, the Cartesian coordinates of all structures have been reported in Supplementary materials. The schematic energy diagram for the present reaction is displayed in Figure 3. Calculated rate constant are displayed in Figure 4. Table 1 gives the total energy, zero point energy, electronic energy and relative energies for all species. Entropy, enthalpies, and free energies are collected in Table 2 and the absolute values of the thermodynamic energies (E, H and G) of relevant species listed in Table S1. The values of the thermodynamic parameters have been calculated at standard conditions (1 atm; 298.15 K). The calculated thermodynamic quantities of reactions have been also tabulated in Table S2. The results of kinetic study are listed in Tables 3 and 4.

3.1. Reactants and pre-reactive complexes

There is evidence that the hydroperoxyl radical reacts with acetaldehyde via a pre-reactive complex [11]. Two complexes are formed between the reactants CH_3CHO and HOO that have been noted as Cr1 and Cr2. The geometries of these complexes are optimized and showed in Figure 1 along with the optimized parameters of the reactants. The most stable complex that is calculated is Cr1. In this complex, we have a six membered-ring structure with C_s molecular symmetry. The interaction of the hydrogen of the hydroperoxyl radical with a lone pair of the oxygen atom of the carbonyl group and simultaneously, the hydrogen atom of acetaldehyde interact with a lone pair of the terminal oxygen atom of HO_2. Therefore, the pre-reactive complex (Cr1) has two intermolecular hydrogen bonding. This observation was also confirmed by an AIM topological analysis of the wave function. This investigation reveals the presence of bond critical points (bcp), located between oxygen of HO_2 radical and hydrogen of acetaldehyde [$\rho = 0.00637$ and $\nabla^2\rho = 0.0216$] and between hydrogen of HO_2 radical and oxygen of acetaldehyde [$\rho = 0.0432$ and $\nabla^2\rho = 0.1048$] and these values for the density of the wave function and the Laplacian are characteristic of hydrogen bond interactions. In addition, a ring critical point was found. The pre-reactive Cr2 complex also has C_s symmetry. As shown in Figure 1, the plane of symmetry bisects the methyl group of acetaldehyde, whereas the HOO moiety is contained in the molecular plane. Also, the hydrogen of hydroperoxyl points toward the oxygen of the carbonyl group and the hydrogen of methyl group interact with the terminal oxygen atom of HOO so that the pre-reactive complex has a seven-membered-ring structure. Moreover, the analysis of the wave function shows two hydrogen bonds and ring critical point. The detailed AIM results for Cr1 and Cr2 were reported in Supplementary materials (Tables S3 and S4). Meanwhile, Table S5 tabulated the rotational constant of Cr1 and Cr2. It should be noted that the similar pre-reactive complexes have been propose for the mechanism of the reaction between acetaldehyde and hydroxyl radical [31].

As shown in Figure 3, there are two pre-reactive complexes for the reaction between the acetaldehyde and hydroperoxyl Radical. These two complexes lead to four different products including P1 ($CH_3COOH + OH$), P2 ($CH_3CHOH + O_2$), P3 ($CH_3CO + H_2O_2$) and P4 ($CH_2CHO + H_2O_2$). Table S2 reports the thermodynamic quantities of the different paths which show that the P1 and P3 paths are the most favorable channels thermodynamically. It is evident that the reaction paths leading to P1 and P2 are through the radical addition mechanism and; P3 and P4 are by hydrogen abstraction mechanism. Following the mechanism details of each path will be explained and discussed.

3.2. Radical addition

There are four channels for radical addition mechanism as:

$$\text{(i)}\ CH_3CHO + HO_2 \rightarrow Cr1 \xrightarrow{TS1} IM1 \xrightarrow{TS2} Cp1 \rightarrow P1(CH3COOH + OH)$$
$$\text{(ii)}\ CH_3CHO + HO_2 \rightarrow Cr1 \xrightarrow{TS1} IM1 \rightarrow P2(CH_3CHOH + O_2)$$
$$\text{(iii)}\ CH_3CHO + HO_2 \rightarrow Cr1 \xrightarrow{TS5} IM2 \xrightarrow{TS6} Cp3 \rightarrow P1(CH_3COOH + OH)$$
$$\text{(iv)}\ CH_3CHO + HO_2 \xrightarrow{TS7} IM3 \xrightarrow{TS8} Cp1 \rightarrow P1(CH_3COOH + OH)$$

Three of them lead to the P1 product while one of them reaches to P2 (see Figure 3). The calculations found six transition states TS1, TS2, TS5, TS6, TS7 and TS8 for the radical addition channel (see Figure 2). TS1 and TS5 are obtained from Cr1 which has a five member ring structure (Cs symmetry). The energy of Cr1 relative to reactants (see Table 1) is in good agreement with that of Da Silva et al. (-9.4 kcal mol^{-1}). The electronic features of TS1 and the mechanism of its creation from Cr1 is proton-coupled electron-transfer (PCET) which has been discussed in details in Ref. [32]. In this mechanism the proton of HO_2 transfers to the oxygen of carbonyl group, which occurs simultaneously with addition of the terminal oxygen of HO_2 to the carbon of acetaldehyde and an intermolecular electron transfer between the two oxygen atoms of the HO_2 moiety [32]. Among the predicted transitions states in this study, TS1 has the lowest activation energy ($\Delta E = -1.518$; see Table 2). The corresponding value, reported by Da Silva et al. is -2.3 kcal/mol. The result of this reaction leads to form the intermediate structure $CH_3HC(OO)OH$ (IM1; see Figure 2) which is a peroxy radical. The presence of this intermediate has been confirmed experimentally and theoretically by Tomas et al. [6] and Da Silva and Bozzelli [10], respectively. The energy of the IM1 in Figure 3 is lower than the related pre-reactive complex (Cr1) and the reactants which are similar to what have been seen by Da Silva and Bozzelli [10]. IM1 can be followed two different channels (i and ii). The first channel goes through TS2 to Cp1 and then to CH_3-COOH + OH (P1) products. The reaction from IM1 to P1 is exothermic by -42.33 kcal/mol and that a hydrogen bond complex, Cp1 (Figure 1) is formed before releasing of the products. The transition state of this reaction has been labels as TS2 in Figure 2. It involves the simultaneous abstraction of hydrogen of carbon atom by the oxygen of the peroxy group with the breakdown of the oxygen–oxygen bond in a highly strengthened (IMG = 1611 cm^{-1}) four-membered ring structure. The value of activation energy (ΔH) relative to IM1 is -38.57 kcal/mol. It should be noticed that this

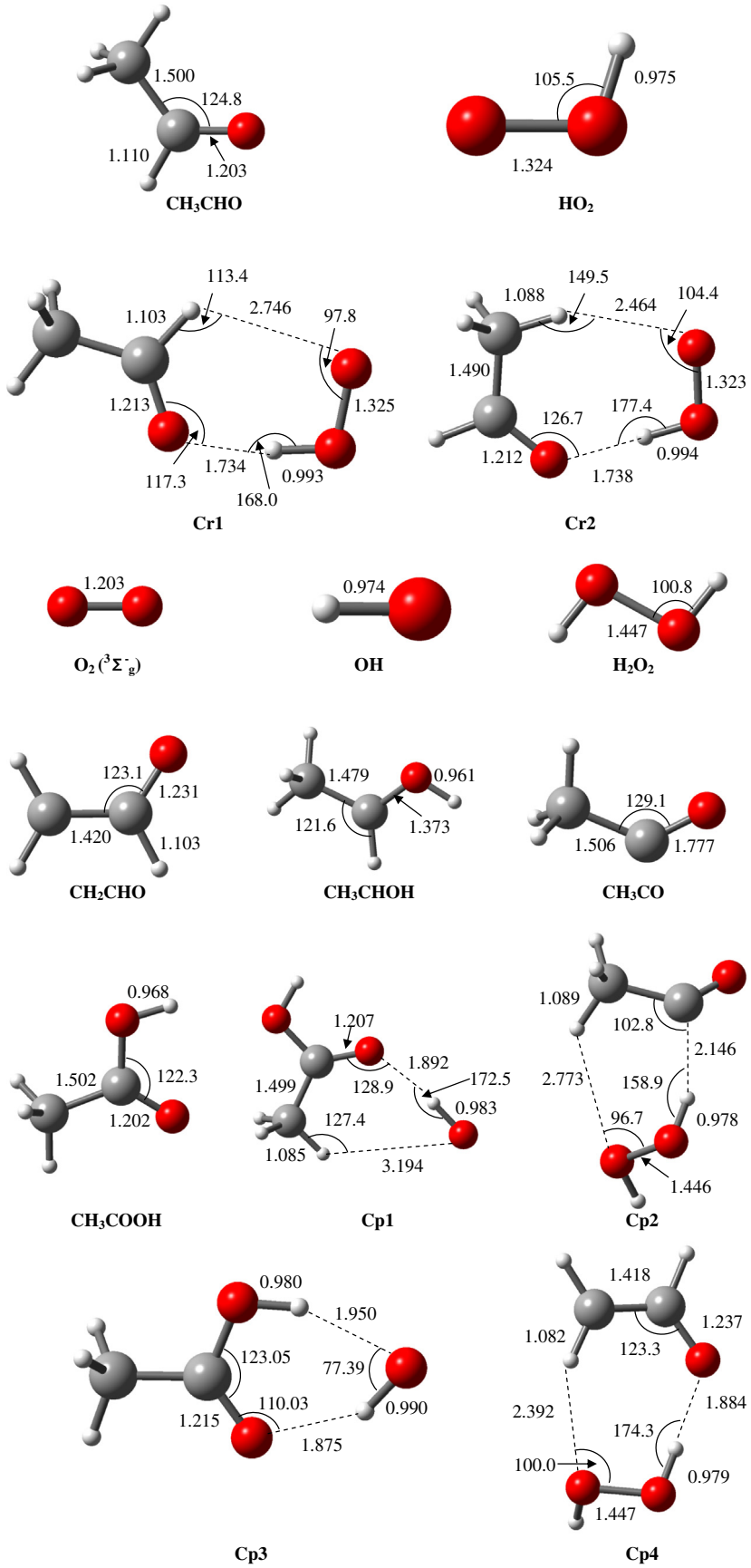

Figure 1. Optimized structures of reactants, pre-reactive complexes, products and pre-product complexes at the B3LYP/6-311++G(3df,3pd) level of theory.

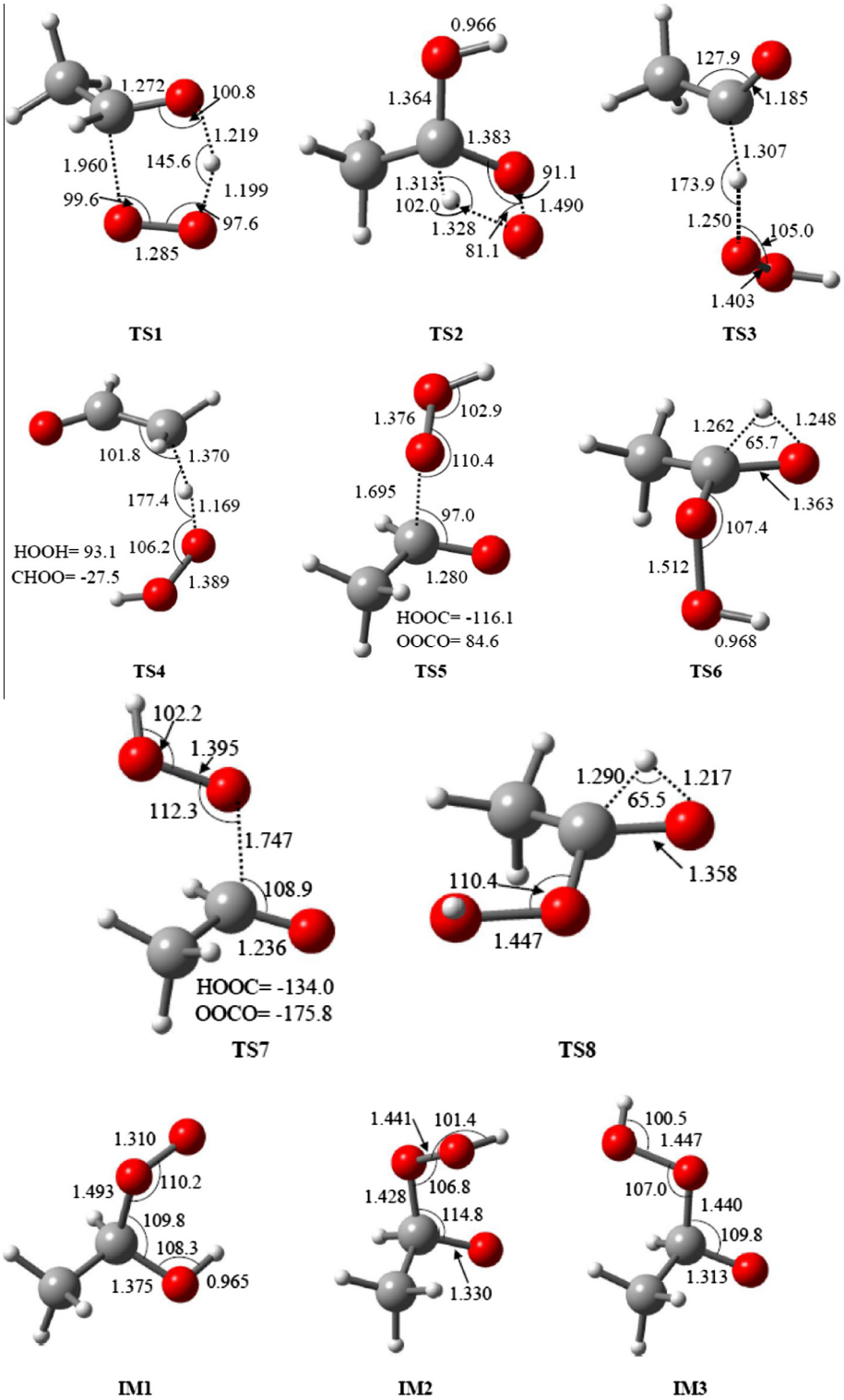

Figure 2. Optimized structures of transition states and intermediates at the B3LYP/6-311++G(3df,3pd) level of theory.

channel has been studied, theoretically, by Anglada and Domingo [5] studied similar channel for the reaction between formaldehyde and HO_2 radical.

The second channel (ii) connects IM1 directly to $CH_3CHOH + O_2$ (P2) which is the most unstable product in this study without passing any transition state. It should be mentioned that the O_2 molecule is in its ground electronic state ($^3\Sigma^-_g$). As seen in Figure 3, this reaction is endothermic (ΔH = 13.32 kcal/mol) which shows that this reaction path is unfavorable from the thermodynamically point of view. During this reaction the bond between carbon and peroxy group is broken and produce oxygen molecule and CH_3-CHOH radical. This channel has also been studied by Da Silva and Bozzelli [10] and observed the dissociation of the IM1 to α-hydoxyethyl and oxygen molecule at high temperatures (1000–2000 K).

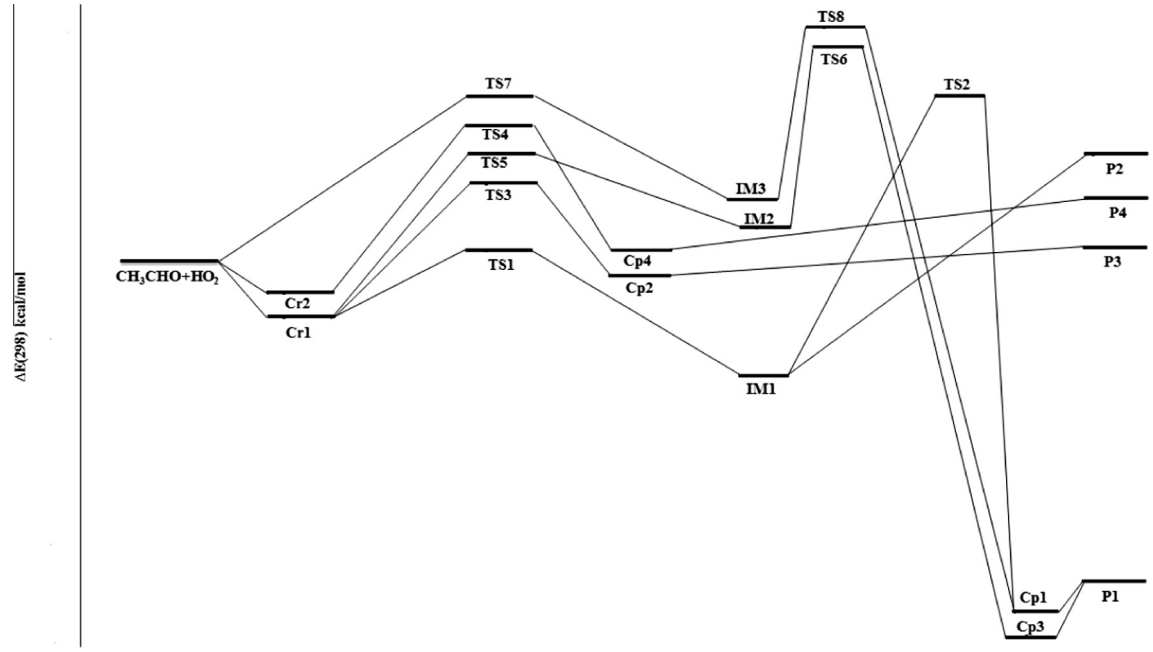

Figure 3. The schematic potential energy surface (PES) of the $CH_3CHO + HO_2$ reaction.

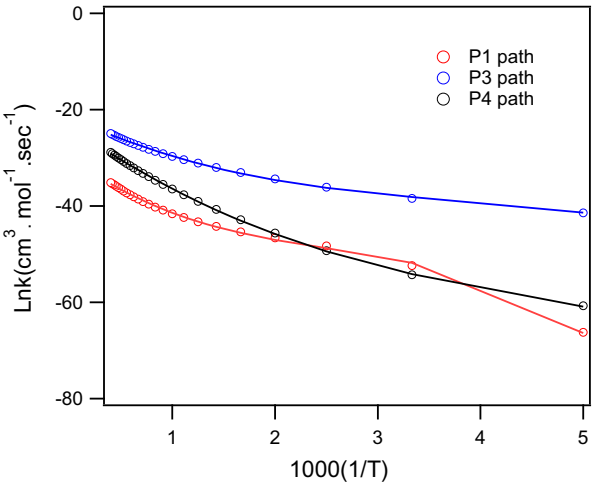

Figure 4. The variation of lnk versus inverse of temperature (T = 200–2500 K) for P1, P3 and P4 paths.

Although, this process is a higher energy process, it is favored by a relatively large pre-exponential factor [10]. It should be mentioned that this reaction path has not been studied by Anglada and Domingo [5] and this path is may be predictable for formaldehyde.

The third and fourth channels (iii and iv) reach to TS5 and TS7 respectively. They are produced by radical addition of HO_2 to the carbonyl bond of CH_3CHO. The calculated values of activation enthalpies of TS5 and TS7 are 18.8 and 20.7 kcal/mol (see Table 2), respectively which are very high and makes these processes unlikely. Similarly, TS7 is produced with the same trend but not from Cr1 (Figure 3). As seen in Figure 2, there is bonding between the carbon of carbonyl group and the terminal oxygen of peroxy radical. The only difference between these two transition states is related to the rotation of OH bond of peroxy. The TS5 is an anti-conformer while TS7 has cis conformation. TS5 and TS7 reaches to intermediate species including IM2 and IM3, reactively. Again, it is evident from Figure 2 that the difference between the structures of IM2 and IM3 is due to the rotation of OH group. TS6 and TS8 (obtained from IM2 and IM3, respectively) leads to pre-products complex including Cp3 and Cp1, respectively.

3.3. Hydrogen abstraction

There are two channels for hydrogen abstraction mechanism as:

$$\text{(i)}\ CH_3CHO + HO_2 \rightarrow Cr1 \xrightarrow{TS3} Cp2 \rightarrow P3(CH_3CO + H_2O_2)$$
$$\text{(ii)}\ CH_3CHO + HO_2 \rightarrow Cr2 \xrightarrow{TS4} Cp4 \rightarrow P4(CH_2CHO + H_2O_2)$$

The structures of TS3 and TS4 have been shown in Figure 2. As seen, there is a difference between them so that in TS3 the hydrogen of carbonyl group goes toward breaking while in TS4 the hydrogen of methyl group is breaking. The geometrical difference between TS3 and TS4 is related to the distance between the transferring hydrogen and carbon atom connected to it. As shown in Figure 2, this distance for TS3 and TS4 are 1.307 and 1.370 Å, respectively because of different hybridization of carbon atoms (TS3 (sp^2); TS4 (sp^3)). The activation energies of TS3 and TS4 relative to the reactants are 6.893 and 5.849 kcal/mol (see Table 2), respectively. The complex products Cp2 and Cp4 have been shown in Figure 1. As seen, Cp2 has six member ring structure while Cp4 is a seven-membered ring containing two hydrogen bonds. The enthalpy change (ΔH) between P3 and Cp2; P4 and Cp4 are 2.722 and 5.661 kcal/mol, respectively. These small values of ΔH and the oxygen–hydrogen and carbon–hydrogen distances, confirms that these complex products easily leads to the products (P3 and P4).

4. Rate constant calculation

Rate constant is a key parameter in kinetic study of reaction that can be calculated from statistical mechanics and its equation is obtained from transition state theory (TST) based on statistical mechanics [33]. For bimolecular reactions, one traditionally uses transition state theory, which requires knowledge of an accurate transition structure so the activation energy is known. The following is a familiar equation for calculating the rate constant for a bimolecular reaction, originally derived from Eyring [34]:

Table 1
Zero-point energies (ZPE), total energy (E_T) and ZPE-corrected energies (E + ZPE) at the B3LYP/6-311++G(3df,3pd) and CCSD(T)/6-311++G(d,p) levels of theory.

Species	ZPE[a]	B3LYP/6-311++G(3df,3pd) E_T	CCSD(T)/6-311++G(d,p) E_T	Relative energies	(E + ZPE)[b]
$CH_3CHO + HO_2$	0.06941	−304.86166	−304.11553	0.00	−304.79225
Cr1	0.07231	−304.87693	−304.13123	−9.85 [−7.74]	−304.80461
Cr2	0.07252	−304.87727	−304.13095	−9.67 [−7.64]	−304.80475
TS1	0.07024	−304.86443	−304.11368	1.16	−304.79418
IM1	0.07596	−304.88425	−304.14179	−16.48	−304.80829
TS2	0.07008	−304.81704	−304.07061	28.19	−304.74696
Cp1	0.07270	−304.95701	−304.21901	−64.93 [−63.67]	−304.88430
P1($CH_3COOH + OH$)	0.07002	−304.97482	−304.20998	−59.27	−304.87779
P2($CH_3COH + O_2$)	0.06944	−304.82742	−304.08226	20.88	−304.21381
TS5	0.07263	−304.83412	−304.08467	19.36	−304.76149
TS7	0.07097	−304.82955	−304.07080	28.07	−304.75857
IM2	0.07384	−304.84995	−304.10811	4.65	−304.77611
TS6	0.06825	−304.80196	−304.05503	37.96	−304.73371
TS8	0.06908	−304.80078	−304.05464	38.20	−304.73170
Cp3	0.07290	−304.96136	−304.22231	−67.00 [−64.92]	−304.88279
IM3	0.07342	−304.84793	−304.10478	6.74	−304.77450
TS3	0.06670	−304.84788	−304.09333	13.93	−304.78118
Cp2	0.07136	−304.86232	−304.11946	−2.46 [−0.92]	−304.79095
P3($CH_3CO + H_2O_2$)	0.06962	−304.85595	−304.11219	2.09	−304.78530
TS4	0.06605	−304.83190	−304.07742	23.91	−304.76584
Cp4	0.07940	−304.85854	−304.11258	1.851 [3.88]	−304.88920
P4($CH_2CHO + H_2O_2$)	0.06896	−304.84676	−304.09991	9.81	−304.77678

[a,b] Values obtained at B3LYP/6-311 + G(3df,3pd). ZPE and E_T (total energy) in hartree and relative energy in kcal/mol. Values in brackets include BSSE corrections.

$$k_{bim} = L\chi \frac{Q^{TS}}{Q_A Q_B} \frac{k_B T}{h} e^{-\frac{E_0}{k_B T}} \quad (4)$$

where χ is the tunneling correction; L is the Avogadro constant; E_0 is the energy barrier between TS and reactants including zero point energy corrections; Q^{TS}, Q_A, and Q_B are the partition functions of the transition structure and reactant species, respectively. The Q parameters for one species is the product of translational, rotational, vibrational, and electronic partition functions, k_B is Boltzmann's constant; and h is Planck's constant.

According to classical mechanics, a particle can cross a potential energy barrier only if its energy is higher than the barrier height, while quantum mechanics predicts that there is a probability for the crossing at lower particle energies. This transmission probability is very sensitive to the particle energy and mass, the barrier height, and the shape of the barrier. The tunneling correction factor is defined as the quotient of the quantum mechanical rate to the classical rate. Although the tunneling process is a multidimensional phenomenon, for simplicity this is treated as a one-dimensional process. Also, one possible cause for a deviation from Arrhenius behavior is quantum mechanical tunneling of reactants through classical barrier which was assumed conservation of vibrational frequencies and moments of inertia of the fragments during the course of reaction. In this study, we used the simplest approach to assess the role of quantum tunneling which is the asymmetric Eckart potential [34] correction to the reaction rate.

The rate constant for unimolecular reaction channel as calculated by RRKM (Rice–Ramsperger–Kassel–Marcus) theory. In RRKM theory, the thermal rate coefficient is obtained by integrating over E from E_0 to infinity of the following equation:

$$k = \int_{E_0}^{\infty} \frac{k_2(E) dk_1(E)[M]}{k_{-1}[M] + k_2(E)} \quad (5)$$

Where k_i, E_0, E, and M are defined based on the Lindemann mechanism for the first order chemical reactions. The various terms of the rate expression are now evaluated using statistical mechanics. In the high pressure limit, RRKM theory reduces to transition state theory and the results of the two theories coincide.

Table 2
Entropies (S), reaction and activation energies (E), enthalpies (H), and free energies (G) at the B3LYP/6-311++G(3df,3pd) level of theory.

Species	$S°$ (e.u.)	$\Delta E°$ (kcal/mol)	$\Delta H°$ (kcal/mol)	$\Delta G°$ (kcal/mol)
$CH_3CHO + HO_2$	117.29	0.00	0.00	0.00
Cr1	88.11	−9.58	−7.85	0.85
Cr2	86.43	−9.21	−7.50	1.05
TS1	75.24	−1.52	−2.35	9.72
IM1	76.66	−14.18	−11.22	0.89
TS2	75.33	28.21	27.35	39.40
Cp1	89.13	−59.24	−57.42	−49.67
$P_1(CH_3COOH + OH)$	111.62	−54.06	−53.55	−51.86
$P_2(CH_3COH + O_2)$	115.07	22.08	2.097	22.11
TS5	77.21	17.87	18.79	30.10
TS7	78.43	20.74	20.75	31.69
IM2	77.14	7.94	9.65	20.97
TS6	78.96	37.46	35.87	47.30
TS8	78.31	38.20	37.06	48.68
Cp3	84.84	−62.56	−57.23	−47.56
IM3	77.32	9.21	10.70	21.97
TS3	88.27	8.86	6.86	15.06
Cp2	93.03	−0.20	1.48	8.25
$P_3(CH_3CO + H_2O_2)$	119.75	3.79	4.20	3.01
TS4	84.64	10.05	5.85	3.84
Cp4	87.06	2.55	3.95	12.32
$P_4(CH_2CHO + H_2O_2)$	117.46	9.94	9.61	8.92

Table 3
Values of rate constants for P1 path at 200–2500 K.

T	K_{eq-Cr1} [a]	k_2 [b]	k_{TS1} [c]	k_{-2} [b]	k_{TS2} [b]	k_T
200	2.38×10^{-18}	13.16×10^{4}	3.14×10^{-13}	2.15×10^{10}	1.17×10^{-6}	1.71×10^{-29}
300	4.49×10^{-21}	6.22×10^{6}	2.79×10^{-14}	8.94×10^{10}	5.82×10^{4}	1.82×10^{-23}
400	2.34×10^{-22}	4.99×10^{7}	1.17×10^{-14}	3.83×10^{11}	3.47×10^{4}	1.06×10^{-21}
500	4.48×10^{-23}	1.80×10^{8}	8.07×10^{-15}	5.27×10^{11}	3.63×10^{5}	5.55×10^{-21}
600	1.62×10^{-23}	4.31×10^{8}	6.99×10^{-15}	6.31×10^{11}	1.80×10^{6}	2.00×10^{-20}
700	8.35×10^{-24}	8.15×10^{8}	6.81×10^{-15}	7.35×10^{11}	6.53×10^{6}	6.05×10^{-20}
800	5.34×10^{-24}	1.33×10^{9}	7.07×10^{-15}	8.44×10^{11}	1.93×10^{7}	1.61×10^{-19}
900	3.91×10^{-24}	1.95×10^{9}	7.64×10^{-15}	9.62×10^{11}	4.90×10^{7}	3.89×10^{-19}
1000	3.15×10^{-24}	2.68×10^{9}	8.43×10^{-15}	1.09×10^{12}	1.11×10^{8}	8.59×10^{-19}
1100	2.71×10^{-24}	3.48×10^{9}	9.43×10^{-15}	1.22×10^{12}	2.28×10^{8}	1.76×10^{-18}
1200	2.44×10^{-24}	4.35×10^{9}	1.06×10^{-14}	1.36×10^{12}	4.34×10^{8}	3.39×10^{-18}
1300	2.28×10^{-24}	5.27×10^{9}	1.20×10^{-14}	1.51×10^{12}	7.74×10^{8}	6.16×10^{-18}
1400	2.18×10^{-24}	6.22×10^{9}	1.36×10^{-14}	1.66×10^{12}	1.30×10^{9}	1.07×10^{-17}
1500	2.13×10^{-24}	7.21×10^{9}	1.54×10^{-14}	1.82×10^{12}	2.10×10^{9}	1.77×10^{-17}
1600	2.12×10^{-24}	8.21×10^{9}	1.74×10^{-14}	1.99×10^{12}	3.23×10^{9}	2.82×10^{-17}
1700	2.13×10^{-24}	9.22×10^{9}	1.96×10^{-14}	2.15×10^{12}	4.79×10^{9}	4.36×10^{-17}
1800	2.15×10^{-24}	1.02×10^{10}	2.20×10^{-14}	2.32×10^{12}	6.89×10^{9}	6.53×10^{-17}
1900	2.20×10^{-24}	1.12×10^{10}	2.47×10^{-14}	2.49×10^{12}	9.61×10^{9}	9.52×10^{-17}
2000	2.26×10^{-24}	1.22×10^{10}	2.76×10^{-14}	2.67×10^{12}	1.31×10^{10}	1.35×10^{-16}
2100	2.33×10^{-24}	1.32×10^{10}	3.08×10^{-14}	2.84×10^{12}	1.73×10^{10}	1.87×10^{-16}
2200	2.41×10^{-24}	1.42×10^{10}	3.43×10^{-14}	3.02×10^{12}	2.23×10^{10}	2.54×10^{-16}
2300	2.50×10^{-24}	1.52×10^{10}	3.80×10^{-14}	3.19×10^{12}	2.82×10^{10}	3.36×10^{-16}
2400	2.61×10^{-24}	1.61×10^{10}	4.20×10^{-14}	3.36×10^{12}	3.48×10^{10}	4.36×10^{-16}
2500	2.72×10^{-24}	1.71×10^{10}	4.64×10^{-14}	3.52×10^{12}	4.19×10^{10}	5.53×10^{-16}

[a] in cm^3 $molecule^{-1}$.
[b] in s^{-1}.
[c] in cm^3 $molecule^{-1}$ s^{-1}.

In this part, the kinetics of the favorable paths of reaction between CH_3CHO and HO_2 radical are studied based on the transition state theory using the RRKM (multi-channel reaction) and TST [33] (one step reaction) theories implemented in the Ssumes [35] and Gpop [36] programs. The rate constant corrected for tunneling by assuming asymmetric Eckart potential [37].

The favorable paths (the paths with the minimum energies) for the reaction, based on the calculations in this work, are P1, P3 and P4. The values of the rate constants for the path P1 has been reported in Table 4 at different temperatures (200–2500 K). In this table the value of K_{eq-Cr1}, $K_{eq-Cr1} = k_1/k_{-1}$, is the equilibrium constant between the reactants and Cr1 where k_1 and k_{-1} are the rate constant for forward and reverse of Cr1 formation from reactants. The total rate constant of the Cr1 → TS1 → IM1 reaction and its reverse has been shown as k_2 and k_{-2} in Table 3, respectively. The rate constant for the reaction (reactant → IM1) is equal to $K_{eq-Cr1} \times k_2$ and has been displayed as k_{TS1} in Table 3. k_{TS2} shows the rate constant for IM1 → TS2 → P1 reaction. Base on RRKM theory, to obtain the overall rate constant (k_T) of the reaction (reactant → P1) at infinite pressure, the product of the rate constants of the forward reactions should be divided to the product of the rate constant of the reverse reactions as this equation $K_{eq-Cr1} \times k_2 \times k_{TS2}/k_{-2}$. It is evident for Table 3 that the reaction between the HO_2 radical and CH_3CHO is relatively slow because of the small value of the rate constant (k_T). Also, it can be seen that the rate constant increases with the increase of temperature. For example, by increasing the temperature from 200 to 2500 K, k_T will be ten thousand times.

Figure 4 shows the variation of the ln k_T versus the inverse of temperature for P1 path. It can be seen that the plot shows a strong non-Arrhenius temperature dependence at the considered temperature range. This behavior is related to the temperature dependence of the pre-exponential factor in the Arrhenius equation. The values of ln k_T for P1 path were fitted in the following equation:

$$\ln k = \ln[A(T)] - \frac{E_a}{RT} \tag{6}$$

where A is the pre-exponential factor which is generally temperature dependent and E_a is the activation energy. Non-Arrhenius equation for the rate constant of P1 path, obtained from the fitting, is defined as:

$$\ln(k) = -29.77 - 2177.7\left(\frac{1}{T}\right) + (4.95 \times 10^{6})\left(\frac{1}{T}\right)^2 - (6.45 \times 10^{8})\left(\frac{1}{T}\right)^3 - \frac{(114500)(\mathrm{J/mol \cdot K})}{RT} \tag{7}$$

The results of the fitting have been shown in Figure 4. It can be seen that the temperature dependence of ln[$A(T)$] is not a linear equation which means that the non-Arrhenius effects are consider-

Table 4
Values of rate constants (in s^{-1}) for P3 and P4 paths at 200–2500 K.

T	k_3	k_4
200	1.01×10^{-18}	4.27×10^{-27}
300	2.09×10^{-17}	2.65×10^{-24}
400	2.06×10^{-16}	3.88×10^{-22}
500	1.15×10^{-15}	1.57×10^{-20}
600	4.35×10^{-15}	2.47×10^{-19}
700	1.27×10^{-14}	2.07×10^{-18}
800	3.07×10^{-14}	1.12×10^{-17}
900	6.48×10^{-14}	4.46×10^{-17}
1000	1.23×10^{-13}	1.42×10^{-16}
1100	2.17×10^{-13}	3.81×10^{-16}
1200	3.57×10^{-13}	8.95×10^{-16}
1300	5.58×10^{-13}	1.89×10^{-15}
1400	8.34×10^{-13}	3.68×10^{-15}
1500	1.20×10^{-12}	6.65×10^{-15}
1600	1.68×10^{-12}	1.13×10^{-14}
1700	2.29×10^{-12}	1.84×10^{-14}
1800	3.05×10^{-12}	2.87×10^{-14}
1900	3.97×10^{-12}	4.31×10^{-14}
2000	5.09×10^{-12}	6.27×10^{-14}
2100	6.42×10^{-12}	8.88×10^{-14}
2200	7.99×10^{-12}	1.23×10^{-13}
2300	9.81×10^{-12}	1.66×10^{-13}
2400	1.19×10^{-11}	2.20×10^{-13}
2500	1.43×10^{-11}	2.87×10^{-13}

able for this path reaction. The calculated activation energy for the P1 path is equal to 114.5 kJ/mol. Table 4 reports the rate constants of P3 (k_3) and P4 (k_4) at different temperatures. The rate constants k_3 and k_4 are related for converting Cr1 → Cp2 and Cr2 → Cp4, respectively. It should be noted that the procedure used for calculating the k_3 and k_4 is similar to that was used for P1 path. As shown in Figure 4, it can be also seen that there is the non-Arrhenius temperature behavior for P3 and P4 paths. Eqs. (6) and (7) demonstrate the Non-Arrhenius equations obtained from the fitting of the rate constants of the P3 and P4 paths at different temperatures, respectively.

$$\ln(k) = -21.44 - 435.21\left(\frac{1}{T}\right) + (2.178\times10^{6})\left(\frac{1}{T}\right)^{2} - (1.88\times10^{8})\left(\frac{1}{T}\right)^{3} - \frac{81035(\mathrm{J/mol\cdot K})}{RT} \quad (8)$$

$$\ln(k) = -23.37 - 175.82\left(\frac{1}{T}\right) + (2.28\times10^{6})\left(\frac{1}{T}\right)^{2} - (1.49\times10^{8})\left(\frac{1}{T}\right)^{3} - \frac{124767(\mathrm{J/mol\cdot K})}{RT} \quad (9)$$

The values of the activation energy for P3 and P4 paths are 81.035 and 124.767 kJ/mol, respectively.

It is also evident for Figure 4 that the Non-Arrhenius effect in P1 path is higher than P3 and P4 paths. In addition, the percent branching of these paths have been listed in Table 4. It is evident from Table 4 that the channel P3 is more favorable than P4 path in the low temperature range considered in this study as a candidate for the hydrogen abstraction channel. The hydrogen abstraction of acyl group (P3) has also been studied by Da Silva et al. [10,38] and the overall rate constant and activation energy of this channel at temperature range of 900–1200 K were reported ($k = 3.01\times1012\exp(-6000/T)\ \mathrm{cm^3\ mol^{-1}\ s^{-1}}$; $E_a = 11.9\ \mathrm{kcal\ mol^{-1}}$). The corresponding results, calculated in this work at the same rang of temperature, are ($k = 1.20\times1010\ \exp(-6520/T)\ \mathrm{cm^3\ mol^{-1}\ s^{-1}}$; $E_a = 12.9\ \mathrm{kcal\ mol^{-1}}$).

As mentioned before, Tomas et al. [6] and Crawford et al. [39] studied, experimentally, the reaction between CH_3CHO and HO_2, separately. Tomas et al. [6] considered IM1 as the final product for this reaction. Their reaction continues with another hydropropoxyl radical which has been not considered in the present study. The calculated rate constant for the formation of IM1 from CH_3CHO and HO_2 ($CH_3CHO + HO_2 \rightarrow IM1$) in this work is $2.79\times10^{-14}\ \mathrm{cm^3\ mol^{-1}\ s^{-1}}$ at 300 K which is comparable with the values of Tomas et al. [6] ($4.4\times10^{-14}\ \mathrm{cm^3\ molecule^{-1}\ s^{-1}}$) and Crawford et al. [39] ($5\times10^{-14}\ \mathrm{cm^3\ molecule^{-1}\ s^{-1}}$). It can be seen that there is a good agreement between theory and experimental results.

5. Conclusions

In this work, quantum chemical calculations were employed to reveal the thermodynamic and kinetic of the important atmospheric reaction between CH_3CHO with HO_2 radical in gas phase. Different structures corresponding to various stationary point on the potential energy surface, leading to $CH_3COOH + OH$, $CH_3CHOH + O_2$, $CH_3CO + H_2O_2$ and $CH_2CHO + H_2O_2$ products, were characterized. Transition state theory along with the RRKM method was employed to calculate the rate constants of different stages in the favorable paths. The calculated rate constants at different temperature for P1, P3 and P4 paths showed the presence of non-Arrhenius temperature behavior. The calculations performed in this work show that the path P1 (radical addition mechanism) is the most favorable from the thermodynamically and kinetically point of view, compared to the other paths. Therefore, the reaction between the CH_3CHO with HO_2 radical mostly produces acetic acid and hydroxyl radical in atmosphere at the temperature range considered in this study. Also, it was shown that the only one path of hydrogen abstraction mechanism (P3) is considerably more probable than the other one (P4), thermodynamically and kinetically.

Acknowledgments

The authors gratefully acknowledge the financial supports of University of Zanjan and Isfahan University of Technology.

Appendix A. Supplementary data

Supplementary data associated with this article can be found, in the online version, at http://dx.doi.org/10.1016/j.cplett.2013.07.065.

References

[1] R. Atkinson, Atmos. Environ. 34 (2000) 2063.
[2] L. Magne, S. Pasquiers, V. Edon, F. Jorand, C. Postel, J. Amorim, J. Phys. D 38 (2005) 3446.
[3] H. Lee, M. Chang, Plasma Chem. Plasma Proc. (2000) 21329.
[4] H. Lee, M. Chang, J. Adv. Oxid. Technol. (2003) 648.
[5] J.M. Anglada, V.M. Domingo, J. Phys. Chem. A 109 (2005) 10786.
[6] A. Tomas, E. Villenave, R. Lesclaux, J. Phys. Chem. A 105 (2001) 3505.
[7] L. Sandhiya, P. Kolandaivel, Struct. Chem. 23 (2012) 1475.
[8] M.T.C. Martins-Costa, J.M. Anglada, J.S. Francisco, M.F. Ruiz-Lopez, J. Am. Chem. Soc. 134 (2012) (1827) 11821.
[9] L. Vereecken, J.S. Francisco, Chem. Soc. Rev. 41 (2012) 6259.
[10] G. Da Silva, J.W. Bozzelli, Chem. Phys. Lett. 483 (2009) 25.
[11] J.V. Michael, D.G. Keil, R.B. Klemm, J. Chem. Phys. 83 (1985) 1630.
[12] A.D. Becke, J. Chem. Phys. 98 (1993) 5648.
[13] C. Lee, W. Yang, R.G. Parr, Phys. Rev. B. 37 (1988) 785.
[14] Y. Li, H.L. Liu, X.R. Huang, D.Q. Wang, C.C. Sun, A.C. Tang, J. Phys. Chem. A 112 (2008) 12252.
[15] K. Fukui, Acc. Chem. Res. 14 (1981) 363.
[16] M. Page, J.W. McIver, J. Chem. Phys. 88 (1988) 922.
[17] C. Gonzalez, H.B. Schlegel, J. Chem. Phys. 90 (1989) 2154.
[18] C. Gonzalez, H.B. Schlegel, J. Phys. Chem. 94 (1990) 5523.
[19] J. Cizek, Adv. Chem. Phys. 14 (1969) 35.
[20] R.J. Barlett, J. Phys. Chem. 93 (1989) 1963.
[21] S.F. Boys, F. Bernardi, Mol. Phys. 19 (1970) 553.
[22] M.J. Frisch et al., Gaussian 03, Revision B.03, Gaussian, Inc., Pittsburgh, PA, 2003.
[23] R.F.W. Bader, Chem. Rev. 91 (1991) 893.
[24] T.A. Keith, AIMAll, Version 12.06.03, TK Gristmill Software, Overland Park KS, USA, 2012. aim.tkgristmill.com.
[25] S.J. Klippenstein, R.A. Marcus, J. Chem. Phys. 87 (1987) 3410.
[26] S.J. Klippenstein, Chem. Phys. Lett. 170 (1990) 71.
[27] S.J. Klippenstein, J. Chem. Phys. 96 (1992) 367.
[28] S.J. Klippenstein, J. Phys. Chem. 98 (1994) 11459.
[29] D.M. Wardlaw, R.A. Marcus, Chem. Phys. Lett. 110 (1984) 230.
[30] D.M. Wardlaw, R.A. Marcus, J. Chem. Phys. 83 (1985) 3462.
[31] J.R. Alvarez-Idaboy, N. Mora-Diez, R.J. Boyd, A. Vivier-Bunge, J. Am. Chem. Soc. 123 (2001) 2018.
[32] S. Olivella, J.M. Anglada, A. Sole, J.M. Bofill, Chem. Eur. J. 10 (2004) 3404.
[33] J.I. Steinfeld, J.S. Francisco, W.L. Hase, Chemical Kinetics and Dynamic, Prentice-Hall, Upper Saddle River, 1989.
[34] H. Eyring, J. Chem. Phys. 3 (1935) 107.
[35] A. Miyoshi, Steady-State Unimolecular Master-Equation Solver (SSUMES), University of Tokyo, 2010.
[36] A. Miyoshi, Gaussian Post Processor (GPOP), University of Tokyo, 2010.
[37] B.C. Garrett, D.G. Truhlar, J. Phys. Chem. 83 (1979) 2921.
[38] D.L. Bauch et al., J. Phys. Chem. Ref. Data 21 (1992) 411.
[39] M.A. Crawford, T.J. Wallington, J.J. Szente, M.M. Maricq, J.S. Francisco, J. Phys. Chem. A 103 (1999) 365.